Vibrational motion of the radical cation C3+ in its degenerate electronic ground state.

Wilfried Meyer, Pavel Rosmus, Weber Thomas

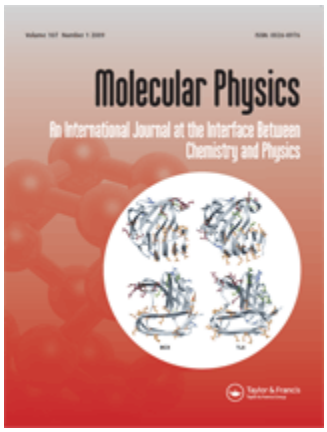

Vibrational motion of the radical cation C_3^+ in its degenerate electronic ground state.

Journal:	*Molecular Physics*
Manuscript ID:	TMPH-2009-0333.R1
Manuscript Type:	Special Issue Paper - In honour of Prof Werner 60th birthday
Date Submitted by the Author:	11-Feb-2010
Complete List of Authors:	Meyer, Wilfried; University of Kaiserslautern, Chemistry Rosmus, Pavel; Universite de Marne la Valee, Laboratoire de Chimie Theorique Thomas, Weber; University of kaiserslautern, Chemistry
Keywords:	electronic structure, molecular vibration, C3
Note: The following files were submitted by the author for peer review, but cannot be converted to PDF. You must view these files (e.g. movies) online.	
c3.new.tex wfredplot.tex c3.new.bib c3.figa.zip c3.figE.zip c3.figA1.zip	

Vibrational motion of the radical cation C_3^+ in its degenerate electronic ground state

Thomas Weber[1], Wilfried Meyer[1] and Pavel Rosmus[2]
[1]*Fachbereich Chemie, Technische Universität Ksaiserslautern, 67653 Kaiserslautern, Germany*
[2]*Laboratoire de Chimie Théorique, Université de Marne la Valée, 77454 Champs sur Marne, France*
(Dated: February 12, 2010)

The cation C_3^+ plays an important role in astrophysical reactions but so far it has not been characterized spectroscopically. Theory has established a complicated degenerate electronic ground state with a conical intersection of D_{3h} structure and three local minima of $D_{\infty h}$ structure. The small isomerization energy is not well determined with estimates ranging from 3 to 7 kcal/mol.

In this paper the first attempt is made to generate a reliable global potential energy surface. The MR-CI method is used to cope with a very strong multi-configurational electronic structure. Including Davidson corrections and complete basis extrapolation, we predict a Jahn-Teller stabilization energy of 1334 cm^{-1}, a pseudorotation barrier of 376 cm^{-1}, a well depth of the linear minima of 289 cm^{-1} and an electronic isomerization energy of 2238 cm^{-1} (6.4 kcal/mol).

An analytical form of the potential surface is used in variational calculations of low-energy vibrational motions which are based on hyperspherical coordinates. Vibronic coupling is treated in a diabatic framework for the J-T region as well as the near-linear region. We find a unique mixture of vibrational states which are either located around the three cyclic minima or the three linear minima, or they are global in the sense that they fill the energy valleys between these minima. Assignments are proposed in terms of local vibrator quantum numbers. Zero point energies in the cyclic global and linear local minima are 1626 cm^{-1} and 1195 cm^{-1}, respectively, i.e. the isomerization energy is reduced by vibrational effects to 1668 cm^{-1} (4.75 kcal/mol).

I. INTRODUCTION

The cation C_3^+ has been intensively investigated since it was suggested that it may play a crucial role in the process of forming larger homonuclear carbon clusters in interstellar space via hydrogenation steps [1]. The room temperature reaction rate of the hydrogen abstraction reaction $C_3^+ + H_2 \rightarrow C_3H^+ + H$ was found abnormally low as compared to the rates of other C_n^+ ion clusters [2, 3] which has been tentatively linked to a cyclic C_3^+ structure. Recent ion trap studies revealed a surprisingly steep increase of the reaction rate down to about 50 K where it suddenly levels off [4]. At this low temperatures even the radiativ association reaction $C_3^+ + H_2 \rightarrow C_3H_2^+ + h\nu$ becomes competitive. So far there is no well-based explanation of this inverse temperature dependence, speculation envisions either a long-living precursor complex or a structural peculiarity of C_3^+ such as very facile bent-to-linear isomerization.

Apart from these reaction rates, there are indeed only very few experimental data available. Coulomb explosion experiments [5] have been interpreted as indicating a cyclic structure in contrast to older theoretical predictions of a linear structure. While early measurements of the first IP of C_3 left a range from 11 to 13 eV [6, 7], the recently measured photoionization efficiency curve of C_3 [8] shows a clear step for vertical ionization at 11.70 $\pm$0.05 eV and in particular a rather long tail to lower energies wich is believed to indicate unresolved vibrational states of a bent C_3^+. However, a firm experimental determination of its structure and a detailed spectroscopic characterization of C_3^+ are still missing.

Sunil et al [9] reported the first careful theoretical investigation of ionization potentials of C_3 and noted a particularly strong role of electron correlation for the properties of (linear) C_3^+. It can be traced to rather low-lying nonbonding $1\pi_g$ orbitals which are not occupied in the Hartree-Fock (HF) configurations of the $^2\Sigma_u^+$ and $^2\Sigma_g^+$ states, $4\sigma_g^2 3\sigma_u 1\pi_u^4$ and $4\sigma_g 3\sigma_u^2 1\pi_u^4$, respectively. They give rise to large left-right correlation via strong admixture of pair excitations into $1\pi_g^2$ or $\sigma_{u,g}1\pi_g$. This results in a reordering of the electronic statess by moving the $^2\Sigma_u^+$ and $^2\Sigma_g^+$ states below the $^2\Pi_u$ state, the lowest at the HF level. It turned out that SD-CI still gave a wrong ordering of states and the Moller-Plesset perturbation series MP_n showed large oscillations of the correlation energies in particular from triple excitations. Only multi reference configuration treatments - MC-SCF as well as MR-CI - produced the correct ordering and a first IP of 11.5 eV in good agreement with the recent experimental value quoted above.

The observation of a complex electronic structure of C_3^+ and the suggestion of a cyclic structure [5] triggered a rush of high-level *ab initio* calculations in which all possible methods and a large number of basis sets were explored, with the main purpose to ascertain the bent-to-linear isomerization energy (which we henceforth abbreviate by ΔE^e). Raghavachari [10] used the quadratic configuration interaction method (QCISD(T)) with a relatively small basis set and was the first to predict a bent $^2B_2$ global minimum with apex angle of 67°. This minimum is only 3 kcal/mol lower than the $^2\Sigma_u^+$ minimum of linear C_3^+ but separated from it by a barrier which rises about 4 kcal/mol above the linear minimum. An imaginary force constant for the asymmetric stretch mode indicated symmetry breaking even at the level of a restricted QCISD(T). Applying a similar basis and the same method, but based on a UHF reference function, Martin et al [11] proposed 1.9 kcal/mol as best estimate

for ΔE^e and stressed that this value would be further reduced by a zero point energy (ZPE) difference of about 0.7 kcal/mol. Grev et al. [12] tried the single reference CI method, exploring substitution levels up to quadruples and various active orbital spaces to conclude that the ΔE^e should be about 4 kcal/mol, however with an uncertainty of $\pm$ 4 kcal/mol. They found a small imaginary bending frequency for the $^2\Sigma_u^+$ state indicating a direct decent to the $^2B_2$ minimum and also report symmetry breaking for the HF wavefunctions of the $^2\Sigma_u^+$ and $^2B_2$ states which prevails for SD-CI.

The newly established singles and doubles coupled cluster method with perturbative triples (CCSD(T)) was applied by Scuseria [13] with a focus on basis set saturation. Using atomic natural orbitals in symmetry-restricted calculations, ΔE^e was found to increase monotonically with basis set size and reached 6.8 kcal/mol for the largest set. The performance of the CCSD(T) was investigated by Watts et al. [14] trying out various schemes for handling triple excitations, including the full CCSDT. They encountered variations up to 5 kcal/mol and concluded that the generally accepted CCSD(T) approximation artificially favors the linear structure by 2.0 kcal/mol. The results for the antisymmetric stretch frequency were indicative for the problems of single-reference methods with C_3^+ : It changed from 1431i for CCSD(T) to 451i for CCSDT but was real for other variants.

Taylor et al. [15] stressed the strong multi-reference character of correlation in the lower electronic states of C_3^+ as the primary cause of the problems. They performed a series of CASSCF/MRCI calculations with a full-valence active orbital space, state-averaged orbital optimization, reference configuration selection with varying thresholds for their coefficients and optionally applying a multireference analogue of the Davidson correction. Their best calculation yielded a ΔE^e value of 5.18 kcal/mol. A critical evaluation of various energy increments and an estimate for the deficiency of their basis set data led them to propose an energy difference of 5.2 kcal/mol as best estimate, with a confidence interval from 4.2 to 6.7 kcal/mol. This nicely includes the estimate of ref. [12] at the lower end and the best calculated value of ref. [13] at the upper end and it has not been challenged since. It should not be overlooked, however, that they encountered imaginary frequencies for antisymmetric stretch of the linear species even at their full-valence CASSCF level.

The problems encountered with all the methods tried seem to have so far prevented any investigation of larger parts of the ground state energy surface. Only harmonic frequencies have been reported in some of the work discussed above, as they come along with geometry optimization. However, for bending and antisymmetric stretch vibrational modes they are of very limited use in view of the obvious strong anharmonicities. Symmetric stretch frequencies for the linear form vary between 1154 cm^{-1} from CASSCF [15] and 1261 cm^{-1} from SDCI [12], not very different from the experimental C_3 frequency of 1225 cm^{-1}. For the bent form, symmetric stretch frequencies reported from well correlated treatments vary between 1590 and 1724 cm^{-1}. The only attempt to provide a global potential energy surface has recently been made by Wang et al. [16]. An analytical expression was derived from a straight application of the many-body expansion theory [17] of polyatomic interaction potentials. The parameters were taken from potential curves of the dissociation products C_2 and C_2^+ and from the harmonic force constants pertaining to the $^2B_2$ global minimum. Since no reference was made to the peculiarities of the electronic structure of C_3^+ this analytical surface can not expected to be really useful.

For the sake of completeness we mention some recent theoretical results which have been generated in the context of experimental work. McAnoy et al. [18] performed single-point CCSD(T) calculations with an aug-cc-pVTZ basis, albeit for B3LYP optimized geometries. While the ΔE^e of 5.7 kcal/mol does fit into the picture of previous work, a rather high barrier of 2.9 kcal/mol is suggested. Fura et al. [19] applied a quite similar but unrestricted scheme to a larger number of ion clusters and reported a rather small ΔE^e of only 1 kcal/molr. Nicolas et al. [8] presented CASSCF/MR-CI potential curves along the bending coordinate while fixing the CC bond length to a value favouring the linear form. Thus, the suggested ΔE^e of 2.2 kcal/mol as well as a flat, suspiciously looking hump may be artifactual.

All these variations in the results for ΔE^e and the transition state barrier indicate that great care has to be taken if a potential surface is to be generated that can be trusted. It is the purpose of the present paper to establish a global potential energy surface (PES) which is reliable up to some lower vibrational levels of linear C_3^+ , i.e. the conformation in which it is most likely formed. Both sheets of the adiabatic PES are obtained from MR-CI calculations in numerical form on a grid that covers all conformations which are accessible within the given energy range (Section II). These data are used to generate an analytical PES suitable for integration with global vibrational basis functions (Section III). A transformation based on a J-T parametrization of the potential in the cyclic region and on the dipole moment matrix in the linear regian provides a PES in diabatic form for efficient account of vibronic coupling (Section IV). Vibrational states are finally obtained from variational calculations wich use hyperspherical coordinates for proper treatment of symmetry requirements and boundary conditions at D_{3h} and $D_{\infty h}$ geometries. They are characterized in terms of their distribution over the cylic and linear domains and in terms of approximate vibrational quantum numbers (Section V).

With respect to analytical fits and vibrational states we follow the technical procedures previously applied to degenerate states of Na_3 [20] and Li_3 [21–23]. Measured vibrational band positions of exited E" states could be reproduced to within 2 cm^{-1} and excellent agreement

with rotational resolved spectra was found. Of course, electronic structure calculations were facilitated by the small number of valence electrons and vibrational motion turned out to be confined to the lower sheets of the E" states. In the more recent analysis of vibrational structures in the $^2E' \leftarrow ^2A_1'$ absorption spectrum of B_3 we arrived at a satisfactory simulation of a spectrum taken in a Ne matrix, but it was difficult to draw conclusions about the accuracy achieved for vibrational levels [24]. In the case of C_3^+ the low-lying conical intersection and the presence of the three local linear minima will substantially complicate the vibrational analysis. Since there is not yet a convincing suggestion of how C_3^+ will eventually be seen spectroscopically we restrict the present investigation to a vibrational analysis of the ground state. It is hoped that this might help understand the unexpected features of its reactivity.

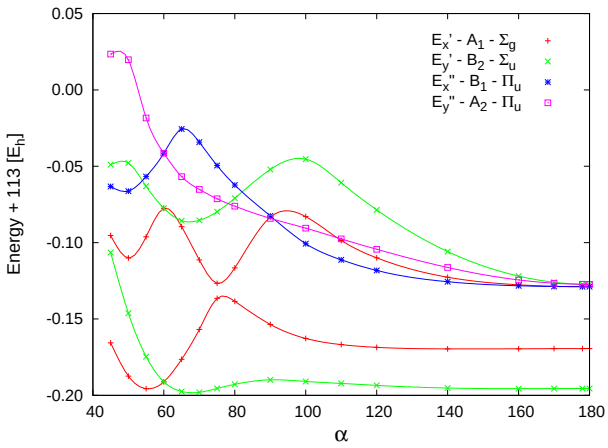

FIG. 1: Cuts of PESs of lower electronic states of C_3^+ along the ground state MEP, from CAS-SCF with basis AVTZ

II. *AB INITIO* ELECTRONIC STRUCTURE CALCULATIONS

From the discussion of the previous investigations of C_3^+ it seems clear that a global PES requires a computational procedure which is based on a multi-configuration reference wavefunction. Lacking a multi-state, multi-configuration coupled cluster program, we have decided to use the multi-reference configuration interaction method (MR-CI) as implemented in the MOLPRO program package [25]. Its particular strength is the efficiency derived from the concept of internally contracted configurations, i.e. singles and doubles substitution operators are applied to the reference function as a whole. This was first formulated by Meyer [26] but developed into an fully operative algorithm and efficiently implemented by Werner and Reinsch [27].

The reference function is obtained from CAS-SCF calculations. The definition of the active orbital space is not trivial in the present case and no perfect solution has been found in test calculations along the minimum energy path (MEP) between the D_{3h} and C_{2v} conformations. The reason is the C-C bond breaking upon opening the apex angle from 60° to 180° which is - as well known for multiple bonds in diatomic molecules, e.g. N_2 [28] - connected with a series of avoided crossings of Rydberg-type with valence-type orbitals and, consequently, crossings of the corresponding configurations. This is seen in Fig. 1 which shows CAS-SCF potential curves of the lower excited states of C_3^+. The optimized orbitals for a preselected set of states therefore undergo rather sudden changes which may affect also the PES of lower-lying states. The resulting humps may be rather large at the CAS-SCF level (e.g. 100-200 cm^{-1} for the lower component of the ground state). They are effectively reduced at the MR-CI level but may still be at a disturbing size of 10-20 cm^{-1}. Since extending the set of states did not improve the situation significantly, we restricted this set to the two components of the ground state which is sufficient to avoid the unphysical symmetry breaking. The avoided crossing of the upper component with the next higher state appears at about 75° of the apex angle, i.e. in a region where the upper component is not significant in itself for the low-energy vibrations. Thus, the effect of the crossing could be diminished by introducing an angle-dependent weighting of the two components which reaches a 1:1 ratio only above 100° . After some experimenting we found as best compromise a set of 13 active orbitals (more precisely 11a', 3a" orbitals in C_s symmetry or $6a_1$, $5b_2$, $2b_1$, $1a_2$ orbitals in C_{2v} symmetry), which is one orbital in excess of the full-valence set used previously. In order to reduce computing expense, an occupation restriction was imposed to the configurations of the reference function in the MR-CI: only two electrons were allowed to occupy simultaneously the four uppermost active orbitals. This restriction has an insignificant effect on the surface even though it may introduce an additional risk for small bumps.

Standard correlation consistent basis sets are used throughout [29]. For the full set of grid points, the cc-pVQZ basis was used [25]. For a significantly smaller subset of points, the VTZ and V5Z basis sets were applied to perform complete basis set extrapolation (CBS) [30]. Since dynamic electron correlation is significantly larger for the more compact cyclic structures than for linear structures, basis set deficiencies are also more serious there. Thus, CBS extrapolation increases ΔE^e by 13%, up from 2125 cm^{-1} to 2401 cm^{-1} . The truncation of the configuration space inherent to a SD-MR-CI expansion has the opposite trend since configuration mixing is stronger for linear structures. Thus, approximately account for higher substitutions by Davidson's correction as implemented in the MR-CI of MOLPRO, lowers ΔE^e by 164 cm^{-1} to our final value of 2238 cm^{-1} . Adding up both extrapolations leads to a bending potential curve which is quite similar to the uncorrected one. Still, the small barrier for bending changes from 359 cm^{-1} to 289

cm^{-1} upon the extrapolations. After corrections, the Jahn-Teller (JT) stabilization energy is predicted as 1334 cm^{-1} and the pseudorotation barrier has a height of only 376 cm^{-1} .

Potential curves along the MEP for apex angles between 50° and 180° are shown in Fig. II. It includes also results from standard CCSD(T) calculations. This

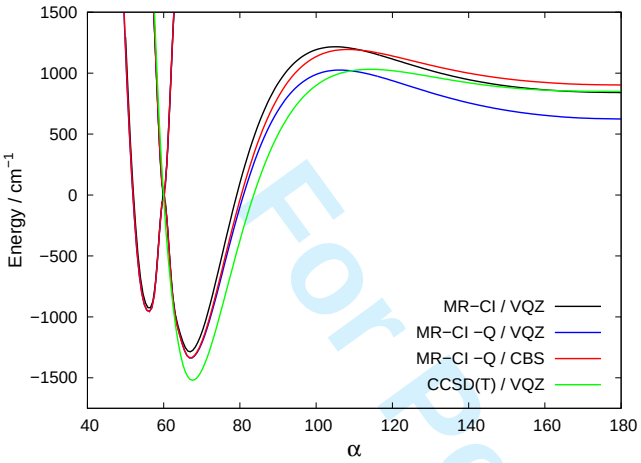

FIG. 2: Cut of ground state PES along the MEP of the lower sheet from fits of MR-CI energies without and with Davidson correction (-Q) or/and CBS extrapolation. Also included is the CCSD(T) PES (cut along an approximate MEP)

method accounts better for dynamical correlation then uncorrected MR-CI but underestimates the effects from near-degenerate configuration mixing. Both differences add up, yielding after CBS extrapolation an ΔE^e isomerization energy of 2660 cm^{-1} and in particular a strongly reduced linear-to-cyclic barrier of only 40 cm^{-1} . We note again that the CCSD(T) treatment converges nicely for C_{2v} geometries (as those of Fig. II) provided the occupied orbitals obey C_{2v} symmetry. But it is difficult to devise a proper one-determinant wavefunction for general C_s geometries: convergence is not stable and may end up in unphysically distorted wavefunctions.

The much discussed question of the stability of the linear minima with respect to asymmetric stretch deformation is elucidated in Fig. 3 and seen to be somewhat academic. The harmonic force constant turns out to be very small indeed: It is weakly positive at equilibrium bond distances but soon changes sign with symmetric bond elongation, i.e. we find a valley-to-ridge transition. The effective force constant related to the fundamental frequency for asymmetric stretch is then largely determined from the positiv quartic force constant.

The molecular constants derived from the MR-CI PES are collected in Tab. II. The structural parameters agree quite well with the better calculations of the literature. Our value for the ΔE^e of 2237 cm^{-1} = 6.4 kcal/mol is within the confidence range proposed by Taylor et al. [15] but close to its upper end. We are certain that the

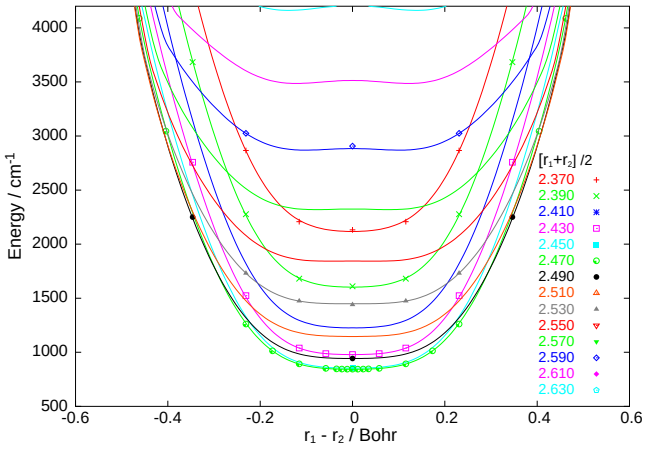

FIG. 3: Cuts of the X_ PES for asymmetric stretch deformation of linear C_3^+; calculated energies (points) and fitted PES (solid lines)

TABLE I: Characteristic points of the X ^{2}E' PES.
Methods and Basis sets: a: this work, MR-CI/cc-pVQZ; b: this work, MR-CI-Q/CBS; c: [10] QCISD(T)/6-31G*; d: [12] CISD(TQ)/TZ2P; e: [13] CCSD(T)/5s4p3d2f1g; f: [15] MR-CI-Q/5s3p2d1f.
Numbers in brackets: ZPE from harmonic frequencies.

		$E+113$ E_h	E_r cm^{-1}	$r_{1,2}$ $\AA$	α °	ZPE cm^{-1}	$\omega_1(a_1)$ cm^{-1}
C_{2v}	a	-0.42535	0	1.322	66.9	1692	1785
min	b	-0.44094	0	1.321	67.1	1626	1780
$^2B_2$	c	-0.40392	0	1.333	67.2	(1811)	1684
	d	-0.29780	0	1.296	71.0	(1759)	1724
	e	-0.43724	0	1.324	67.8		
	f	-0.32590	0	1.324	68.0	1675	1612
C_{2v}	a		357	1.391	55.9		
sadd	b		376	1.391	55.8		1760
D_{3h}	a		1278	1.358	60.0		
min	b		1334	1.358			1792
C_{2v}	a		2487	1.308	104.7		
trans	b		2526	1.308	110.1		1465
	c		2432				
	f		2026				
$D_{\infty h}$	a		2120	1.303	180.0	1251	1190
min	b		2237	1.303		1195	1188
$^2\Sigma_u^+$	c		1051	1.318			
	d		1400	1.283			1261
	e		2383	1.307			
	f		1372	1.314			1154
$^2\Sigma_g^+$	b	T_v	6035				

barrier between linear and bent structures is real, but it is difficult to qualify the accuracy of the 289 cm^{-1} obtained, given the large absolute amounts of CBS and Davidson extrapolations of together about 4700 cm^{-1} .

III. ANALYTICAL REPRESENTATION OF POTENTIAL ENERGY SURFACES

MR-CI calculations as just described have been performed for a grid of non-redundant conformations defined by varying the bond lengths in steps of $\Delta r = 0.05$ Bohr, starting from r = 2.56 Bohr, which is close to r at the D_{3h} geometry with minimum energy, and stopping only after the relative energy exceeded 4000 cm^{-1} above the D_{3h} minimum. With some extra points for bending from linear conformations, this amounted to 250 grid points.

As outlined in section V, the variational calculation of vibrational states involves basis functions that are global in the sense that they span the complete space of the cyclic hyperspherical coordinates θ and ϕ , e.g. harmonic functions of ϕ for pseudorotation. Numerical integration of the potential then requires substantial extension beyond the ranges covered by the grid of the electronic structure calculations. Therefore, we like to have the potentials in an analytical form which is well-behaved everywhere. Moreover, since finite basis sets are used which do not allow a vibrational wavefunction to be exactly zero over finite ranges in coordinate space, we have to make sure that the potential does nowhere assume very large values, including the ranges where two C atoms come very close to each other.

In previous applications to A_3 molecules (with JT distorted potentials) we found it convenient to base an analytical expression on the three bond distances since they are most directly related to bonding forces. In order to further adapt the coordinates to the typical shape of bonding potentials, we introduced 'Morse coordinates' defined as $\tilde{r} = (1 - exp(-\beta(r - r_o)))/\beta$ [31]. This transforms a Morse potential into a parabola with a finite range for positive $\tilde{r}$ and usually allows to represent a bonding potential by a low-order polynomial of $\tilde{r}$. As compared to functions of the apex angle, the steep C_3^+ potentials around 60° are widened and the shallow potentials above 130° are compressed. Thus, β has to be chosen with care so that bending forces can be accounted for also in the linear domain. For the present case we found $\beta = 0.90$ suitable.

The coordinates $\tilde{r}_i$ are combined to form symmetry-adapted coordinates in the usual form:

$$\tilde{r}_a = (\tilde{r}_1 + \tilde{r}_2 + \tilde{r}_3)/\sqrt{3}, \quad (3.1)$$

$$\tilde{r}_x = (2\tilde{r}_3 - \tilde{r}_1 - \tilde{r}_2)/\sqrt{6} \ , \tilde{r}_y = (\tilde{r}_1 - \tilde{r}_2)/\sqrt{2} \quad (3.2)$$

$$\tilde{r}_e = (\tilde{r}_x^2 + \tilde{r}_y^2)/\sqrt{2}, \ \tilde{\phi} = \arctan(\tilde{r}_y/\tilde{r}_x) \quad (3.3)$$

Symmetry is solely carried by functions of ϕ : $\cos(k\tilde{\phi}), \sin(k\tilde{\phi})$ form a pair of E′ species if (k mod 3)$\neq 0$, otherwise they are $A_1' + A_2'$ species. Since the adiabatic PES belong to the A_1' representation, the following linear ansatz for the potential is appropriate:

$$V = \sum_{ijk} v_{ijk} \ \tilde{r}_a^i \ \tilde{r}_e^j \ \cos(3k\tilde{\phi}) \quad (3.4)$$

$$i, j, k = 0, 1, 2, .. \ ; \ i + j \leq n \ ; \ k \leq k_{max}(j) \quad (3.5)$$

$\tilde{r}_e$ is by definition non-negative and is zero only for D_{3h} geometries. At these points, the two components of an E′ state PES are smooth continuations of each other if taken as functions of $\tilde{r}_x$ and $\tilde{r}_y$ due to the fact that they are eigenfunctions of a regular Hamiltonian. Thus, the ansatz above can describe both components with a single set of v_{ijk} if the range of $\tilde{r}_e$ is simply extended to negative values, which then correspond to the upper component PES. In the close neighborhood of $\tilde{r}_e = 0$, v_{ijk} should vanish for $3k > j$ but we only enforce this for $j = 1$. Admittedly, such a one-center polynomial expansion, which worked very well for our previous cases Li_3 and Na_3, is somewhat under stress in the present case where linear geometries matter which have little to do with the conical intersection. In order to ensure sufficient flexibility, we adopted the pragmatic choice of $k \leq 0, 1, 4$ for $j \leq 1, j = 2, j \geq 3$, respectively. The linear ansatz has the obvious advantage that it can easily handle a large number of parameters. It has been preferred over a non-linear fit in terms of the elements of a 2x2 diabatic potential matrix because the upper potential has less quality then the lower. In the present case we have chosen n=8 and $i, j \leq 7$. The total number of terms then amounts to 132. It should be noted that powers of up to 7 in a polynomial expansion are acceptable here because the relevant ranges of $\tilde{r}_a$ and $\tilde{r}_e$ are effectively limited to little more than 1 by the Morse transformation, and extended extrapolation is regularized as described below.

For a sensible least-squares fit the input energies should be weighted according to their relevance. We have chosen the weight function $w(e) = (1 + e/e_0)^{-2}$, where $e = E - E_{min}$, i.e. squares of errors of energy differences are minimized for $e < e_0$ but squares of relative errors for $e > e_0$. Above a certain threshold, $e > e_{max}$, the weight is further reduced by the linear cut-off factor $(2 - e/e_{max})$ and it is set to zero above $2e_{max}$. We have chosen $e_0 = 3000$ cm^{-1} and $e_{max} = 5000$ cm^{-1} , respectively. Around $\alpha = 75°$ a small ridge in the error surface was observed (see discussion in previous chapter) and the weights were reduced to half in that region. The final result comes with a rms error of 4.5 cm^{-1} for fitting the weighted MR-CI energies while the MR-CI-Q energies are fitted with an rms error of 2.9. (The Davidson correction reduces the ridge just mentioned.) Largest deviations amount to less then 15 cm^{-1} . The quality of the fit can also be judged by inspection of Fig. 3 for the most critical region around linear C_3^+ .

We need to deal with the fact that there are large regions of conformation space for which the PES is not controlled by calculated energies and for which the polynomial fit may go wild. Extending the grid does not help since the range of the fit can not easily be extended

without loss of quality in the relevant region. Therefore, the analytical fit needs to be regularized in the regions which are beyond the grid but are accessed by (our) vibrational basis functions. The transformed coordinates $\tilde{r}_a$ and $\tilde{r}_e$ are quite convenient for simple regularizations [20–22, 24, 31]: It is usually possible to determine an ellipsoidal cut-off boundary with respect to a reference point $\tilde{r}_{ao}, \tilde{r}_{eo}$ which encloses all regions where the PES is low and well represented by the fit. Beyond this boundary the PES may be defined with reference to its values at the boundary or close to it. E.g., if the boundary is defined by requiring

$$D^2(\bar{r}_a, \bar{r}_e) = d_a \bar{r}_a^2 + d_e \bar{r}_e^2 + 2 d_{ae} \bar{r}_a \bar{r}_e =! \ \bar{r}_{cut}^2 \qquad (3.6)$$

where $\bar{r}_a = \tilde{r}_a - \tilde{r}_{ao}$ and $\bar{r}_e = \tilde{r}_e - \tilde{r}_{eo}$, the external potential may simply be derived by radial scaling of the coordinates $\bar{r}_a, \bar{r}_e$ whith $t = \bar{r}_{cut}/D(\bar{r}_a, \bar{r}_e)$:

$$E(\tilde{r}_a, \tilde{r}_e, \phi) = E(\bar{r}_a t + \tilde{r}_{ao}, \bar{r}_e t + \tilde{r}_{eo}, \phi)(2 - t^2) \qquad (3.7)$$

This scheme has been chosen here. In addition, the potential is not allowed to exceed an energy E_{max}, chosen here as 14000 and 19000 cm^{-1} for lower and upper surface, respectively. It has been made sure that the calculated vibrational energies are not affected by reasonable changes of all of these parameters.

IV. VIBRONIC COUPLING

In the region of the Jahn-Teller well there is significant vibronic coupling. In adiabatic framework the electronic coupling factor $< \Phi_2^a | \partial / r \partial \phi | \Phi_1^a >$ has a pole at the conical intersection, $r \rightarrow 0$, which has to be removed by the vibrational factor $< \chi_2^a | \partial / r \partial \phi | \chi_1^a >$. For practical reasons, among them program limitations, we prefer a diabatic framework in which the vibronic coupling turns into simple potential coupling. Diabatic electronic states are the specific combinations of the two adiabatic states which have minimal dependense on the angle ϕ. Applying a 2x2 rotation matrix the two adiabatic PESs V_-^{ad}, V_+^{ad} from the MR-CI calculations turn into the diabatic 2x2 matrix PES

$$2V^d = V_+^{ad} + V_-^{ad} + (V_+^{ad} - V_-^{ad}) \begin{pmatrix} \cos\delta & \sin\delta \\ \sin\delta & -\cos\delta \end{pmatrix}$$

where δ is twice the angle for rotating the wavefunctions. The diabatic wavefunctions may be chosen to be identical to the adiabatic ones, $\delta = 0$, at the C_{2v} geometries linked to $\phi = 0$. In the cyclic region around the conical intersectioni, the angle δ can be determined from the familiar expansion of the Hamiltonian in a power series of the polar deformation coordinate r [32, 33]. Since the diabatic wavefunctions Φ_x^d, Φ_y^d form a pair of E′ symmetry, their Hamiltonian matrix elements generate the representation $A_1' \oplus E'$ and may be approximated up to cubic terms in r by

$$\begin{aligned} H_{xx} + H_{yy} &= a_2 r^2 + a_3 r^3 cos(3\phi) \qquad (4.8) \\ H_{xx} - H_{yy} &= e_{13} r \ cos(\phi) + e_2 r^2 cos(2\phi) \\ H_{xy} &= e_{13} r \ sin(\phi) - e_2 r^2 cos(2\phi) \end{aligned}$$

where H_{xy} abbreviates $< \Phi_x^d | H | \Phi_y^d >$ and $e_{13} = e_1 + e_3 r^2$. Diagonalization provides the rotation angle δ as

$$\tan(\delta) = \frac{sin(\phi) - sin(2\phi) \ re_2/e_{13}}{cos(\phi) + cos(2\phi) \ re_2/e_{13}} \qquad (4.9)$$

The expansion coefficients a_n, e_n obtained from a fit of the adiabatic potentials in the J-T region lead to the function $\delta(\phi)$ shown in Fig. 4. Note that $\delta = \phi$ not

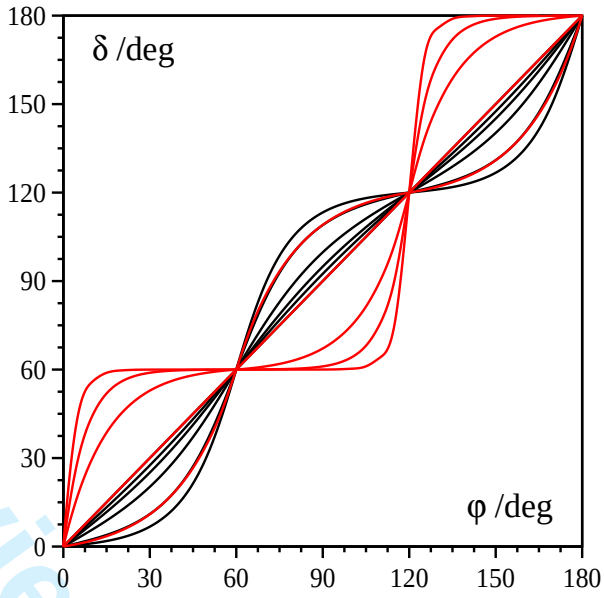

FIG. 4: Rotation angle δ as function of ϕ. Black curves: J-T region , α 60-15-105°; Red curves: linear domain, α = 105-15-180°

only in the linear J-T region but generally at the angles $\phi = n\pi/3$, n=0,1,.., i.e. for all C_{2v} geometries. This has also to be required for a consistent continuation of $\delta(\phi)$ beyond the J-T well.

At the other ends of the bending potential valleys, for linear C_3^+ the separation of the surfaces is 6032 cm^{-1} , much larger than the vibrational energies considered there. Still, vibronic coupling is not negligible for asymmetric stretch motion due to a strong coupling between two diabatic states correlating to $^2\Sigma_u^+$ and $^2\Sigma_g^+$, respectively, which is obvious from the shape of the asymmetric stretch potential, Fig. 3. As asymmetric stretch is always described by the angle ϕ, diabatization is again a matter of defining $\delta(\phi)$. The pertinent quantity is the derivative $(\partial\delta/\partial\phi)_0$ since only small ranges of ϕ around the C_{2v} geometries are probed. (For linear structures the

turning points are below 4° for $v_3 = 0$). The rotation angle has been determined from the matrix elements of the dipole moment operator under the assumption that their changes are solely due to changing mixtures of the diabatic states upon asymmetric stretch. We are led to the relation

$$\tan(\delta) = \Delta\mu/\mu_{12} \qquad (4.10)$$
$$\Delta\mu = |\mu_{11}(\phi) - \mu_{22}(\phi) - (\mu_{11}(0) - \mu_{11}(0))|/2$$

This procedure seems validated by the facts that $\mu_{12}^2 + \Delta\mu^2$ is nearly independent of ϕ and that the resulting diabatic potential has nearly quadratic diagonal elements with a nearly linear coupling element. In Fig. 5 the diabatization procedure is illustrated for linear geometries but the picture changes little for apex angles down to about 120°. Remarkable large values of $\delta/\phi \approx 17$ are obtained which are somewhat difficult to reconsole with the requirement that $\delta \to \phi$ for $\phi \to n\pi/3$. After some experimenting we have settled at an exponential approximation for $\pi/3 - \delta$. This modeling, indicated by dashed curves in Fig. 5, does not affect the vibrational levels, however. The function $\delta(\phi)$ is also shown in Fig. 4. The effect of the vibronic coupling is quite substantial for the zero-point energy of the asymmetric stretch mode: In the linear 1-D model, see Fig. 5, this energy is increased by about 13% or 85 cm^{-1} . After averaging over symmetric stretch and bending motions, there remains a shift of 65 cm^{-1} for low vibrational states that populate linear structures, as compared to the states that populate cyclic structures. Note that the level $v_3 = 1$ is hardly changed so that the fundamental transition is reduced by 85 cm^{-1}.

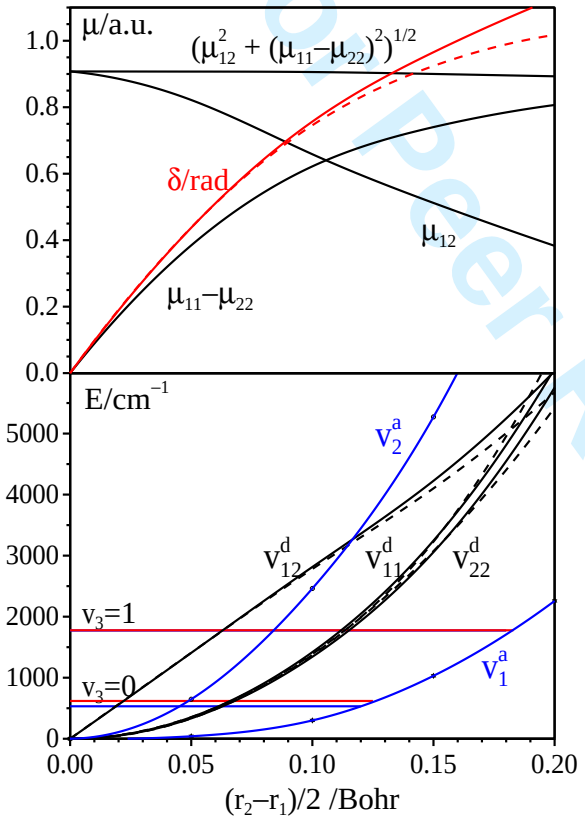

FIG. 5: Transformation to diabatic frame for asymmetric stretch deformation of linear C_3^+ . Upper panel: Dipole moment matrix elements and rotation angle. Lower panel: Adiabatic and diabatic potentials; vibrational levels from uncoupled adiabatic and coupled diabatic treatment.

V. CALCULATION OF VIBRATIONAL STATES

We employ hyperspherical coordinates for ease of taking into account symmetry and proper boundary conditions for cyclic motions. For three equal masses they may be defined by expressing the squares of interatomic distances as [34] (k=1,2,3)

$$r_k^2 = 3^{-1/2}\rho^2(1 + \sin\theta\cos(\phi + \epsilon_k)) \; ; \; \epsilon_k = k2\pi/3. \quad (5.11)$$

where the hyperspherical radius ρ determines the size of the molecule, $\sin\theta$ gives the strength of deformation and ϕ describes the pseudorotation motion around points of D_{3h} symmetry. With this definition $\theta = 0, \pi$ correspond to equilateral geometries (D_{3h}) and $\theta = \pi/2$ to linear ones ($D_{\infty h}$, $C_{\infty v}$), $\phi = 0, \pm 2\pi/3$ gives isosceles triangles (C_{2v}).

For convenient visualization of the actual motion with changing ϕ it is useful to note the relations

$$R = 3^{-3/4}\rho \; \cos(\theta/2) \; ; \; r = 3^{-3/4}\rho \; \sin(\theta/2) \qquad (5.12)$$

where R is the distance of the atoms from the center of mass in the D_{3h} reference geometry and r is the polar radius for the motion around this reference point, see Fig. 6. We shall use (r,ϕ) as coordinates for 2-D plots

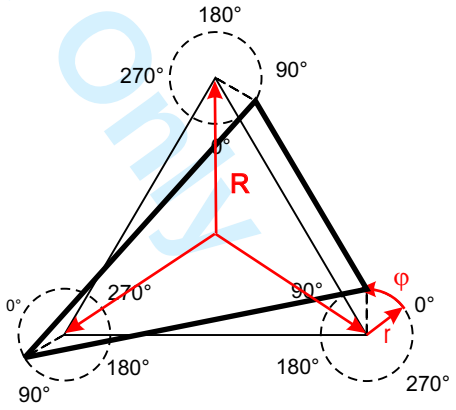

FIG. 6: Pseudorotation motion by varying ϕ with constant ρ, θ or R, r, respectively. Shown is the situation for $\phi = \pi/3$

of the PES and vibrational wavefunctions. Of course, the coordinate surface of the plots should contain the MEP. The latter is close to a pure bend, i.e. $r_1 = r_2 = \rho^2(1-0.5\,\sin\theta)$ constant. Actually, ρ increases somewhat less than this along the MEP and is nearly constant close to $\theta = 0$. It is approximated rather well by defining

$$\rho'^2 = \rho^2[2-(\sin^2\theta + a^2)^{1/2}]/(2-a)\ ;\ a = 0.1885 \quad (5.13)$$

and requiring $\rho' = \text{const}$. Fig. 7 shows contour lines of the lower component PES in a $(\rho', \theta\ ;\ \phi = 0)$ 2-D cut, verifying this relation. Fig. 8 displays contour lines for the 2-D surface $(r, \phi; \rho' = \rho'_0)$. One recognizes the typical structure of a JT potential with its central cone, three equivalent minima separated only by small barriers and three rather narrow valleys along C_{2v} deformations towards linear conformations which are reached at the circular boundary. Note the large coordinate space which is not accessible for its highly repulsive potential. With a strongly anharmonic potential as the one shown in Fig.s 7 and 8, a variational treatment of the vibrational motion is mandatory. Based on the hyperspherical kinetic energy operator introduced by Johnson [34], efficient procedures for the calculation of the Hamiltonian have been devised and implemented by Carter and Meyer [35, 36]. This implementation was originally designed for vibrational and rovibrational states on a single adiabatic PES with geometric phase boundary conditions 0 or π, respectively, but it has more recently been extended by Carter to handle also two electronic states in a diabatic framework. This latter version is applied here since the upper component of the E′ ground state has to be taken into account if vibrational states are investigated that reach out to linear conformations.

The particular strength of our scheme is the tailoring of the vibrational basis functions to fit the given potential. The full-dimensional basis set is generated from lower-dimensional sets by a sequence of contractions based on the eigenfunctions of appropriate parts of the kinetic energy operator and corresponding effective potentials. The effective potentials are defined as lower-dimensional minima of the full-dimensional potential surface and ensure that the basis functions cover adequately all energetically accessible regions of the coordinate space while effectively excluding the regions with high potentials. The primitive 1-D functions are taken to be Morse functions for the radius ρ, Jacoby polynomials for the angle θ and harmonic functions $\cos(m\phi), \sin(m\phi)$ with integer or half-integer modulus m for the angle ϕ . Two-dimensional contracted functions may either be defined for the θ -ϕ subspace or the ρ -θ subspace. Primitive functions as well as contracted functions and their derivatives are represented on a grid and Gauss integration is used for the Hamiltonian. In the present calculations we have used the following sets of primitive and contracted (numbers in parenthesis) functions: ρ : 28(16), θ : 60(54), ϕ : 132(78), ρ -θ (69). The dimension of the Hamiltonian matrices were

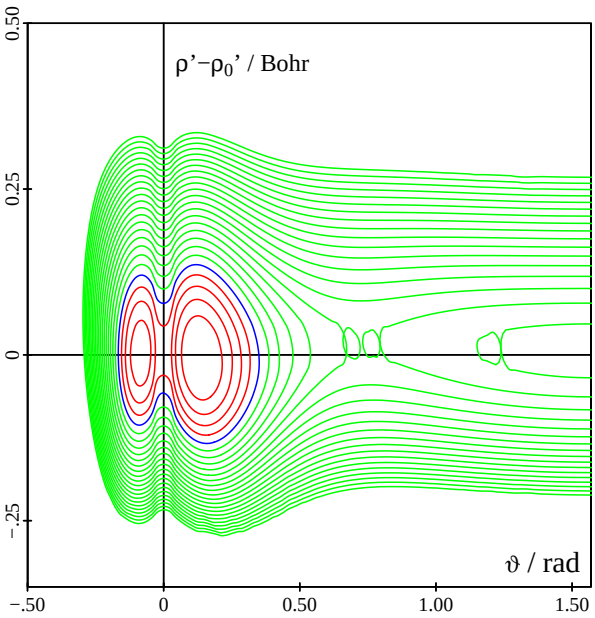

FIG. 7: Contour map of the X_ PES in the ρ'/ϑ plane for $\phi = 0$ with increments of 250 cm^{-1} . Blue line at lowest energy of conical intersection, red lines below, green lines above this energy, respectively.

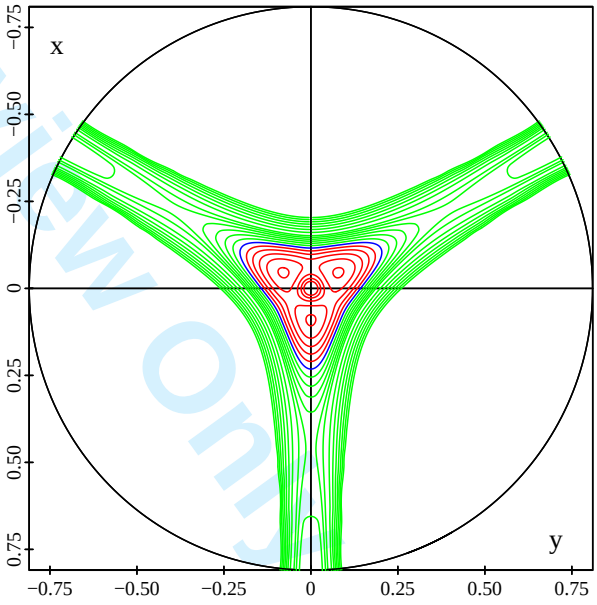

FIG. 8: Contour map of the X_ PES in the r/ϕ polar plane for ρ'=const., i.e. including the MEP of equ. 5.13. The polar radius r is given in equ.5.12 and shown in Fig. 6. Increments are 250 cm^{-1} up to 1250 cm^{-1} and 500 cm^{-1} beyond. Blue line at zero energy = lowest energy of conical intersection; red lines below, green lines above zero energy, respectively.

1850 for A′ symmetries and 3700 for the E′ symmetry, respectively.

The vibronic wavefunctions are symmetry-adapted products of electronic and vibrational wavefunctions. Since the coordinates ρ and θ are not affected by any symmetry operation, vibrational symmetry is determined only by the factor-functions of the coordinate ϕ : The pairs $(\cos(m\phi), (-)^l \sin(m\phi))$ are e′ symmetry species if l = (2m modulo 3) $\neq$ 3, otherwise they generate a_1' and a_2' species, respectively [35, 36]. (The phase factor $(-)^l$ is required to ensure identical representation matrices of C_3 rotations; l is defined to allow for half-integer values of m required in the adiabatic frameA.) As customary, small case letters are used for the symmetry species of vibrational functions. With the diabatic electronic wavefunctions Φ_x, Φ_y one finds the following four species of vibronic wavefunctions:

$$\begin{aligned}
\Psi_{A1} &= \Phi_{Ex}\chi_{e_x} + \Phi_{Ey}\chi_{e_y} \\
\Psi_{Ex} &= \Phi_{Ex}(\chi_{ex} - \chi_{a1}) + \Phi_{Ey}(\chi_{ey} + \chi_{a2}) \\
\Psi_{Ey} &= -\Phi_{Ex}(\chi_{ey} - \chi_{a2}) + \Phi_{Ey}(\chi_{ex} + \chi_{a1}) \\
\Psi_{A2} &= \Phi_{Ex}\chi_{ey} - \Phi_{Ey}\chi_{ex} \qquad (5.14)
\end{aligned}$$

These symmetry species provide the only exact classification of vibronic states. The calculated vibronic energy levels are collected in Tab. V and are displayed in Fig. V. As the shape of the bending potential suggests, we find three groups of vibrational states. The first group, labeled by index b in Tab. V, starts lowest in energy and is confined to strongly bent regions around the conical intersection and the J-T minima. The second group, labeled by l, should appears above energies of 1870 cm^{-1} and is localized in the linear domain. The third group, labeled by g, is global in the sense that the barrier at about 2200 cm^{-1} is overcome and both regions are visited. A further characterization of the vibrational states may be attempted in terms of approximate quantum numbers. For group b states they may be derived by reference to the limiting case of a very high pseudorotation barrier, for which the states are superpositions of the three equivalent states of vibrators localized in the three deep wells. The states can then be labeled by the usual quantum numbers for small-amplitude vibration of a bent molecule. This situation is signaled by near degeneracy of pairs of E′ and A_1' states. The other limiting case, a very low barrier, lends itself to quantum numbers of a free internal rotation and is signaled by near degeneracy of pairs of A_1' and A_2' states. Comparison of the low-energy A_1'-E′ splittings of 201 and 285 cm^{-1} , respectively, with the first A_2'-A_1' splitting of 605 cm^{-1} indicates that the first option is more adequate. Although the pseudorotation barrier of only 376 cm^{-1} seems rather low, a quite effective separation of the three wells is caused by the fact that the saddle point region is rather narrow in bending direction (see Fig. II). Indeed, the lowest A_2' state, which heavily populates the saddle point region, lies as much as 806 cm^{-1} above the ground state. Thus, group b states are assigned with vibrational quantum numbers

TABLE II: Calculated vibrational energy levels (in cm^{-1}) and local vibrator assignments.

A_1'		E'		A_2'	
E	$v_1v_2v_3$	E	$v_1v_2v_3$	E	$v_1v_2v_3$
201	000 b	0	000 b		
966	010 b	681	010 b		
		1245	001 b	806	001 b
1571	020 b	1377	020 b		
1821	100 b	1596	100 b		
1869	000 l	1820	030 b		
2011	030 b	1869	000 l		
		1962	011 b	1806	011 b
2015	020 l	2014	020 l		
2141	040 l	2130	040 l		
2227	070 g	2154	070 g		
2311	080 g	2252	080 g		
2428	090 g	2277	110 b		
2555	110 b	2329	002 b		
2565	0x0 g	2386	090 g		
2658	002 b	2499	0x0 g		
2735	0x0 g	2637	0x0 g		
		2741	021 b	2333	101 b
2894	0x0 g	2794	0x0 g		
		2885	101 b	2569	021 b
		2956	031 g	2935	111 b
		2971	111 b	3002	001 l
		3002	001 l	3110	003 b
3064	100 l	3064	100 l		
3075	0x0 g	3071	120 b		
		3161	021 l	3161	021 l
3173	120 b	3170	0x0 g		
3258	120 l	3194	200 b		
3281		3258	120 l		

(v_1, v_2, v_3) for symmetric stretch, bend and asymmetric stretch modes of a C_{2v} vibrator, respectively. A particular set of such quantum numbers shoul appear twice, that is in E′ and A_1' symmetry for v_3 even but in A_2' and E′ symmetry for v_3 odd. Within such a pair, the energy order E' < A'$_1$ and E' > A'$_2$, respectively, is usually observed. However, this assignment becomes less and less stringent ar higher energies as different local vibrators interact across the pseudorotaton barrier. From the energies given in Table II one derives frequencies for fundamental transitions of 1596-1620 , 681-765 and 1245 cm^{-1} for symmetric stretch, bent and antisymmetric stretch modes, respectively.

In the case of group "l" states one finds E′+A′ pairs which are exactly degenerate because the three components around $\phi = \epsilon_k$, k=1-3, correspond to conformations with different center atoms which do not interact at all.

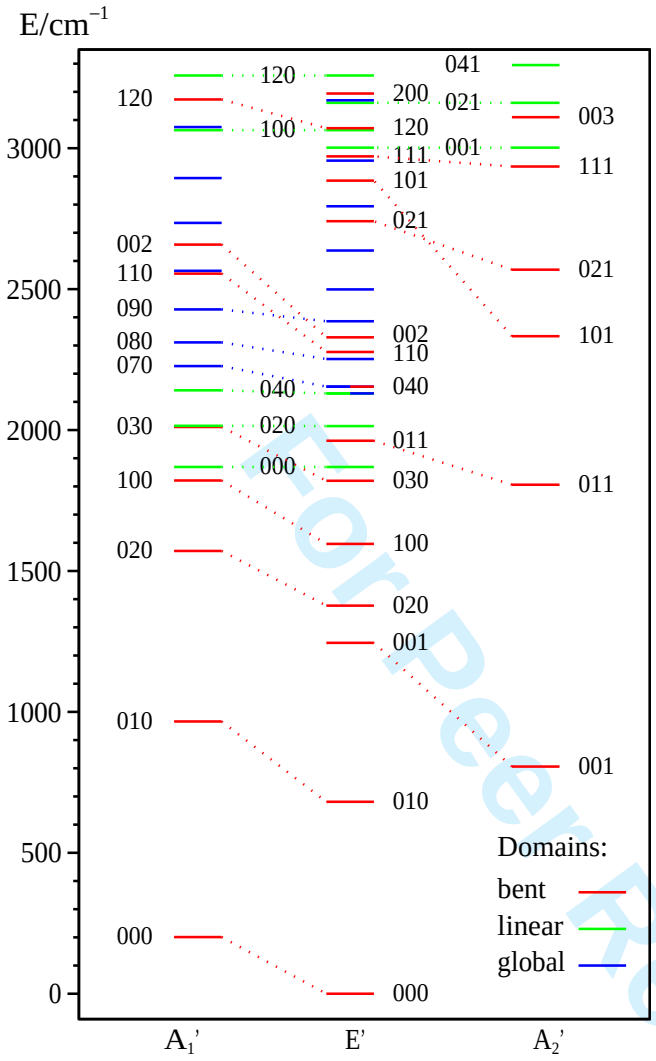

FIG. 9: Vibronic energy levels for XC_3^+ . States with bent (b), linear (l) and global (g) domains indicated in red, green and blue, respectively. Tentative assignment by local vibrator quantum numbers (v_s, v_b, v_{as}); related E-A pairs linked by dotted lines.

Vibrational quantum numbers as used above apply even better to these states but it should be noted that states with v_2 odd do not appear in a rotation-free calculation. We observe only a short progression, $v_2 = 0, 2, (4)$, of low-energy bending vibrations with a fundamental frequency of only 73 cm^{-1} (level distance 146 cm^{-1}), which is due to the broad barrier of 289 cm^{-1} at at $\alpha = 110°$. The levels $v_2 = 4$ at 272 and 261 cm^{-1} , respectively, show already a small splitting from interactions with group b vibrations. The first excitations of symmetric and antisymmetric stretch modes appear with energies 1195 and 1133 cm^{-1}, respectively, above the lowest linear level. (The latter value differs by -25 cm^{-1} from the result of the linear 1-D model for vibronic coupling, which is due to vibrational averaging.) Short bending progressions start with these excitations.

Finally, group g states spread rather evenly over cyclic and linear domains. The vibrational motions appear as 1-D bending vibrations within the three energy valleys, with rather regular interconnections in the cyclic region. (Quantum mechanics appears to effectively suppresses chaotic vibrational motion in the energy range under consideration here.) The states are simply denoted by the number of nodes along the minimum energy path (not double-counting the nodes as in the linear case). The average spacing between consecutive levels is around 110 cm^{-1} , but interactions with the pure cyclic and/or pure linear modes of similar energy cause significant variations. The assignment of quantum numbers becomes more and more questionable with increasing energy but the grouping according to domains turned out rather definite. The assignment has been carried out by applying small diagnostic step potentials and monitoring the resulting shifts of the energy levels. Of course, contour plots of the vibrational wavefunctions have been illuminating and very helpful in this regard.

Selected low-energy vibrational wavefunctions are displayed in figures 9 - 11. For an are adequately representation of global motions the wavefunctions are shown for the $(r,\phi;\rho_0')$ surface as used for the potential in Fig. V. Since it appeared difficult to produce comprehensive pictures of the diabatic wavefunctions, we have transformed them to adiabatic ones. Only the component at the lower surface is shown since there is little population of the very narrow upper adiabatic surface. Note that the nonadiabatic wavefunctions are double-valued with a sign change for the second full period of ϕ. The plots show only the period -π to π and indicate by a bold black line the cut where the wavefunction continues smoothly on the other sheet. As to the symmetry assignment please note that we do not invoke the double group notation. Thus, adiabatic electronic states are considered of A′ symmetry and the symmetry species of adiabatic vibrational states are identical to that of the vibronic states. The lowest vibrational state then has E′ symmetry and shows only a single node over the 4π period ($j_{psr} = 1/2$) while the lowest A_1' and A_2' states have three nodes ($j_{psr} = 3/2$). The latter resides pretty much on top of the pseudorotation barrier. Plots for the $\rho - \theta$ plane have been instructive for the assignment of vibrational quantum numbers but are not shown here.

The vibrational analysis provides a vibronic value for the isomerization energy of $\Delta E^{ev} = 1668$ cm^{-1} (4.75 kcal/mol). The significant difference of 570 cm^{-1} to the purely electronic value of $\Delta E^e = 2238$ cm^{-1} results from the reduction of the ZPE from 1626 cm^{-1} for the cyclic ground state to the vibrational energy of the lowest linear state of only 1195 cm^{-1} , which is due to much weaker bending and antisymmetric stretch potentials.

FIG. 10: Vibronic states of A_1' symmetry.

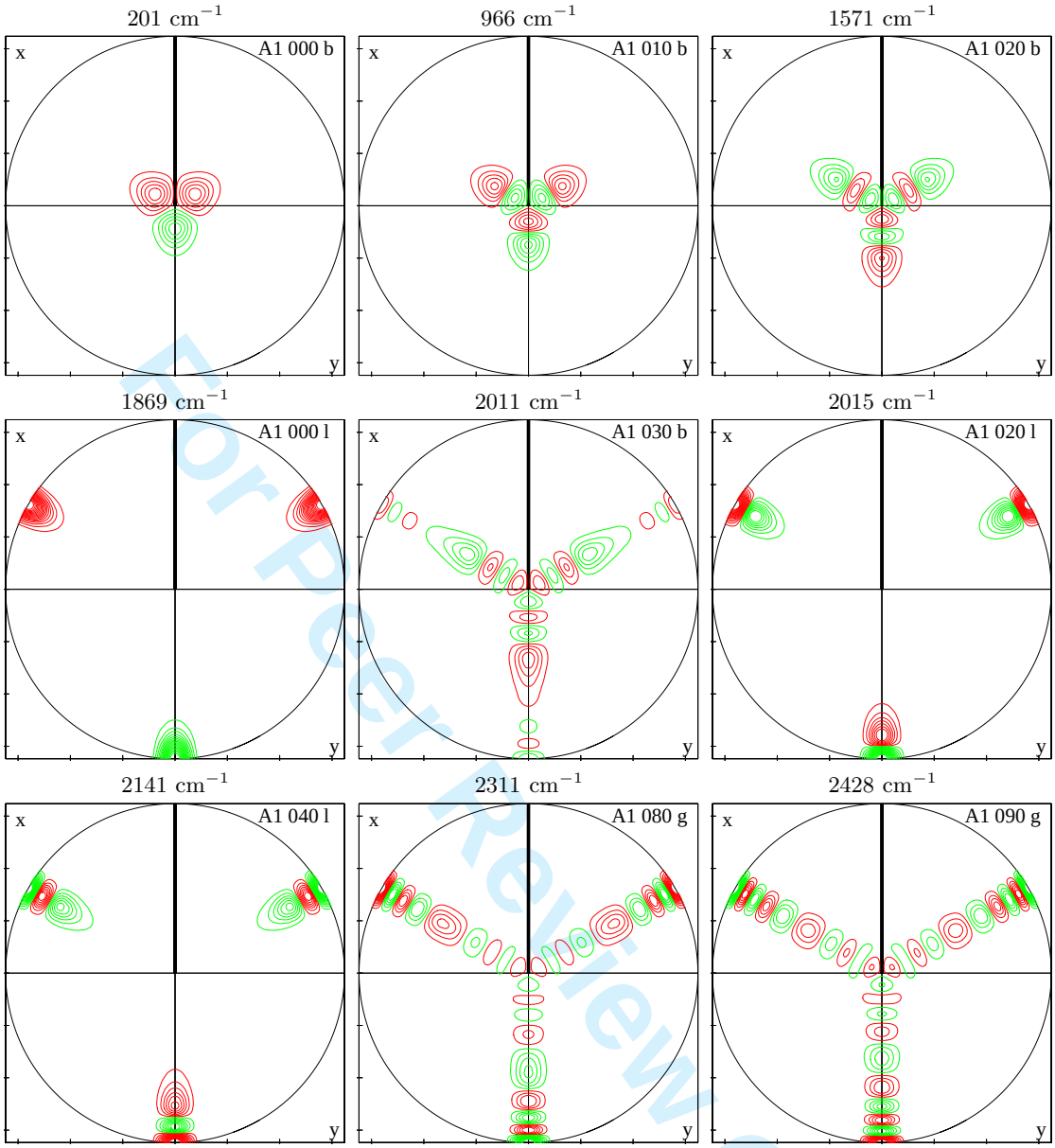

FIG. 11: Vibronic states of A_2' symmetry

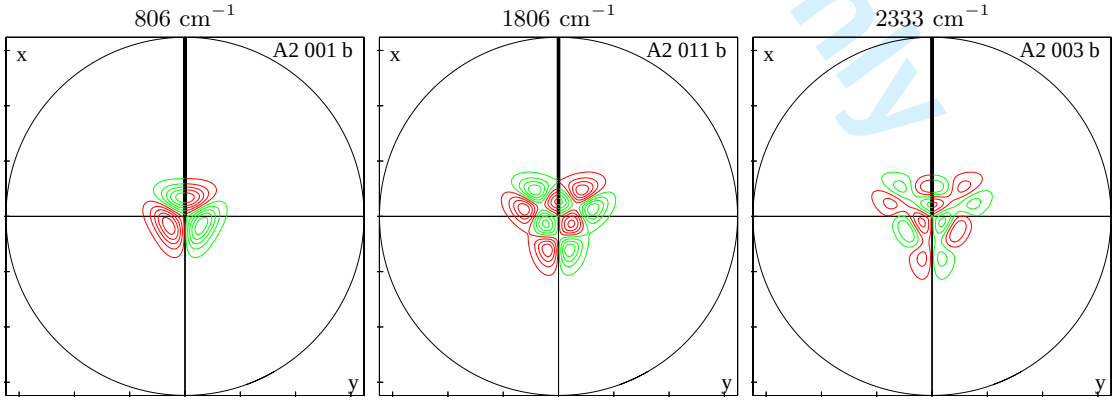

FIG. 12: Vibronic states of E'_y symmetry

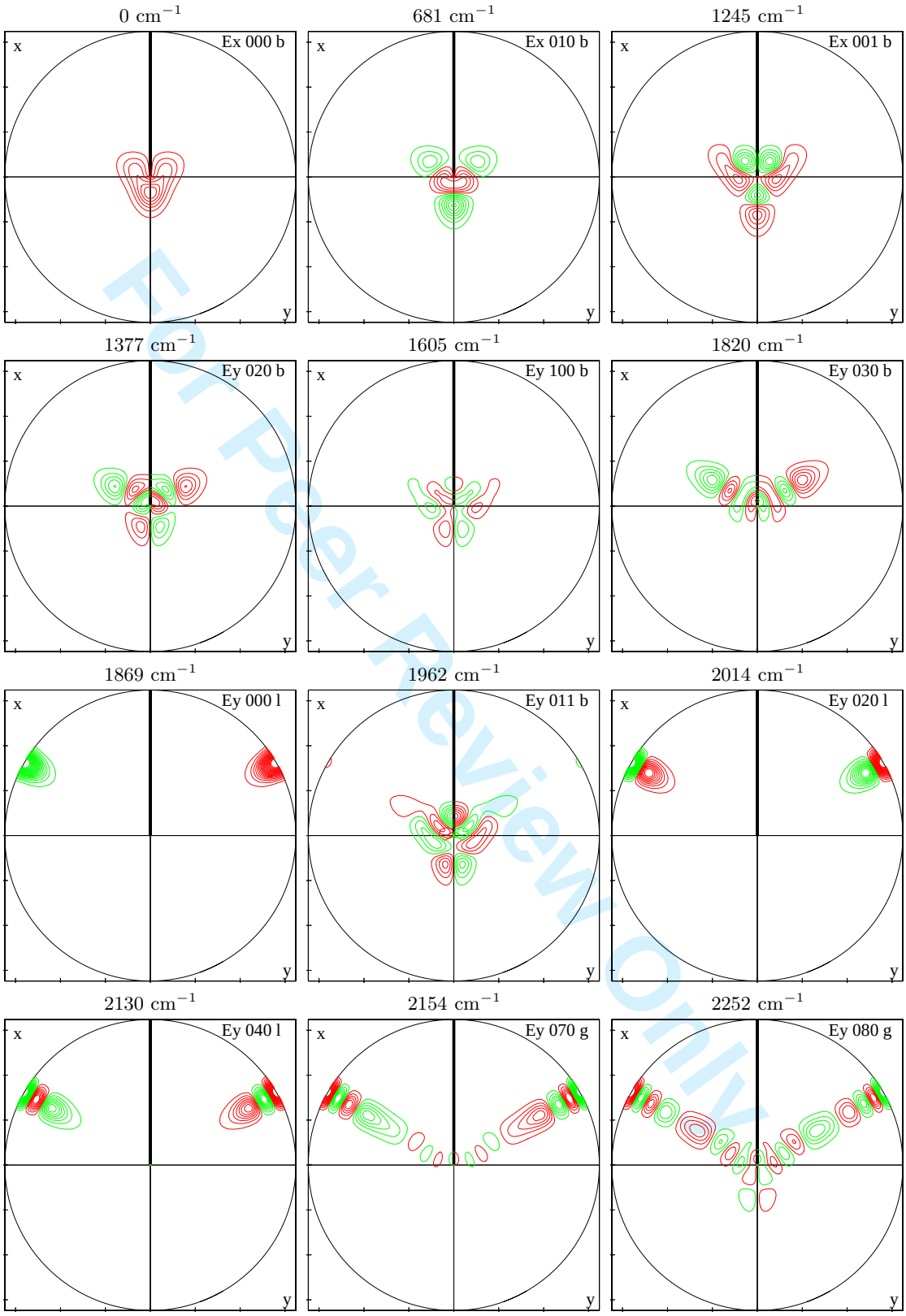

VI. CONCLUSIONS

We have presented a first attempt to generate a reliable global potential energy surface for the electronic ground state of C_3^+. The internally contracted MR-CI method proved to be adequate to deal with the strong multi-configurational character of the electronic structure. A large one-electron basis and beyond full-valence active orbital space as well as extrapolations to complete basis and complete configuration space are believed to support a rather uniform accuracy of about ± 1 kcal/mol for the lower sheet of the potential surface. The electronic isomerization energy $\Delta E^e$is calculated as 2238 cm^{-1} (6.4 kcal/mol), cyclic and linear structures appear separated by a transition state barrier of only 290 cm^{-1}.

The variational calculations of vibronic states take full account of strong vibronic coupling in the cyclic (J-T) and the linear domains of the vibrational motion and are converged to better than 1 cm^{-1}. The complex manyfold of low-energy (< 3000 cm^{-1}) states could be classified according to local motions in the cyclic or the linear domains or global motions connecting all low-energy parts of the PES. A more detailed characterization has been attempted in terms of quantum numbers of local vibrators. The vibrational analysis shows that The isomerization energy is reduced by vibrational effects to the vibronic value of 1626 cm^{-1} (4.75 kcal/mol), due to a rather low ZPE in the linear domain.

The present work is focused on the electronic ground state because of the substantial problems we encountered whith the accurate determination of the upper state wavefunction beyond the J-T region. Work is in progress to derive reliable transition moments for simulation of spectra which may be helpful for identifying C_3^+ spectroscopically.

In a final remark we like to address again the low reaction rate for $C_3^+ + H_2 \rightarrow C_3H^+ + H$ and the puzzle of its inverse temperature dependence mentioned in the introduction. No new options seem to emerge from the knowledge of potential surface and vibrational manyfold of C_3^+ : Only one vibrational level, the A_1' level at 202 cm^{-1}, is subject to temperature dependent population but its structure hardly differs from the ground vibrational state. More information is required on the ionic collision complex. Some exploratory calculations have revealed the following situation: Multipole Coulomb and induction forces form a van der Waals complex with several local minima, the deepest of which is bound by about 3500 cm^{-1} . On the one hand, it may be stabilized with respect to the entrance channel by internal vibrational redistribution. On the other hand, it is separated from the reactive channel by a barrier which rises up to about the educt energy - our calculations are not yet conclusive for the sign of the small difference in energy. This barrier may well explain the low reaction rate at room temperature and maybe even its inverse temperature dependence because the decay channel to the educts is effectively closed at low energies by rotational energy redistribution. Work is in progress to map out the van der Waals potential well and accurately locate the barrier to the reaction channel.

[1] H. Suzuki, Astrophys. J. **272**, 579 (1983).
[2] S.W. McElvany, B.I. Dunlap and A. O'Keefe, J. Chem. Phys. **86**, 715 (1987).
[3] D.K. Bohme and S. Wlodek, Int. J. Mass Spectrom. Ion Processes **102**, 133 (1990).
[4] I. Savic and D. Gerlich, Phys. Chem. Chem. Phys **7**, 1026 (2005).
[5] A. Faibis, E.P. Kanter, L.M. Tack, E. Bakke and B.J. Zabransky, J. Phys. Chem. **91**, 6445 (1987).
[6] J. Drowart, P. Burns, G. DeMaria and M. Inghram., J. Chem. Phys. **31**, 1131 (1959).
[7] F. Kohl and C. Stearns, J. Chem. Phys. **52**, 6310 (1970).
[8] C. Nicolas, J. Shu, D.S. Peterka, M. Hochlaf, L. Poisson, S.R. Leone and M. Ahmed, J. Am. Chem. Soc. **128**, 220 (2006).
[9] K.K. Sunil, A. Orendt, K.D. Jordan and D. Defrees, Chem. Phys. **89**, 245 (1984).
[10] K. Raghavachari, Chem. Phys. Lett. **171**, 249 (1990).
[11] J.M.L. Martin, J.P. Francois and R. Gijbels, J. Chem. Phys **93**, 5037–45 (1990).
[12] R. Grev, I. Alberts and H. Schaefer III, J. Phys. Chem. **94**, 8744 (1990).
[13] G.E. Scuseria, Chem. Phys. Lett. **176**, 27 (1991).
[14] J.D. Watts, J.F. Stanton, J. Gauss and R.J. Bartlett, J. Chem. Phys **94**, 4320 (1991).
[15] P.R. Taylor, J.M.L. Martin, J.P. Francois and R. Gijbels, J. Phys. Chem. **95**, 6530 (1991).
[16] R. Wang, Y. Sheng, C. Yang and Z. Zhu, THEOCHEM **587**, 25 (2002).
[17] K.S. Sorbie and A. Murrel, Mol. Phys. **29**, 1387 (1975).
[18] A. McAnoy, S. Dua, D. Schröder, J. Bowie and H. Schwarz., J. Chem. Soc., Perkin Trans. 2 p. 1647 (2002).
[19] A. Fura, F. Tureček and F.W. McLafferty, Int. J. Mass Spectrom. **217**, 81 (2002).
[20] H. von Busch, V. Dev, H.A. Eckel, S. Kashara, J. Wang, W. Demtröder, P. Sebald and W. Meyer, Phys. Rev. Lett. **81**, 4584 (1998).
[21] H.G. Krämer, M. Keil, C. Suarez, W. Demtröder and W. Meyer, Chem. Phys. Lett. **299**, 212 (1999).
[22] M. Keil, H.G. Krämer, A. Kudell, M. Baig, J. Zhu, W. Demtröder and W. Meyer, J. Chem. Phys. **113**, 7414 (2000).
[23] W. Meyer, M. Keil, A. Kudell, M. Baig, J. Zhu and W. Demtröder, J. Chem. Phys. **115**, 2590 (2001).
[24] M. Wyss, E. Riaplov, A. Batalov, J.P. Maier, T. Weber, W. Meyer and P. Rosmus, J. Chem. Phys **119**, 9703–9709 (2003).
[25] H.J. Werner, P. Knowles and Others, *MOLPRO: a package of ab initio programs, version 2008.1,* 2008.
[26] W. Meyer, in *Methods of Electronic Stucture Theory*,

edited by H.F. Schaefer III, Chap. 11 (Plenum Plublishing Corporation, N.Y., 1977), p. 413.
[27] H.J. Werner and E.A. Reinsch, J. Chem. Phys. **76**, 3144 (1982).
[28] D. Spelsberg and W. Meyer., J. Chem. Phys. **115**, 6438 (2001).
[29] T. Dunning, J. Chem. Phys. **90**, 1007 (1988).
[30] K.A. Peterson, R.A. Kendall and T.H. Dunning, J. Chem. Phys. **99**, 1930–44 (1993).
[31] W. Meyer, P. Botschwina and B. Burton, J. Chem. Phys. **84**, 891 (1986).
[32] W. Moffitt and A. Liehr, Phys. Rev. **106**, 1195 (1957).
[33] G. Herzberg and H. Longuet-Higgins, Discuss. Faraday Soc. **35**, 77 (1963).
[34] B.R. Johnson, J. Chem. Phys. **73**, 5051–8 (1980).
[35] S. Carter and W. Meyer, J. Chem. Phys. **93**, 8902 (1990).
[36] S. Carter and W. Meyer., J. Chem. Phys. **100**, 2104 (1993).